IET Microwaves, Antennas & Propagation

Research Article

IET Journals
The Institution of Engineering and Technology

Synthesis of open structures starting from closed-cross-section waveguide devices

ISSN 1751-8725
Received on 20th October 2019
Revised 25th March 2020
Accepted on 9th July 2020
doi: 10.1049/iet-map.2019.0879
www.ietdl.org

Giuseppe Torrisi[1], Ornella Leonardi[1], Giorgio Sebastiano Mauro[1,2], Luigi Celona[1], Gino Sorbello[1,3] ✉

[1]Istituto Nazionale di Fisica Nucleare - Laboratori Nazionali del Sud, Via S. Sofia 62, Catania, Italy
[2]Dipartimento di Ingegneria dell'Informazione, delle Infrastrutture e dell'Energia Sostenibile, Università degli Studi Mediterranea di Reggio Calabria Salita Melissari, 89124 Reggio Calabria RC, Italy
[3]Dipartimento di Ingegneria Elettrica, Elettronica e Informatica, Università degli Studi di Catania, Viale Andrea Doria 6, 95125, Catania, Italy
✉ *E-mail: gino.sorbello@unict.it*

Abstract: This study presents a new methodology, based on the field modal expansion theory, to derive and analyse millimetre wave (mm-wave) 'open' cross-sections structures starting from standard closed cross-section design. The method is of great interest since W-band open devices offer many advantages over traditional closed structures in terms of risks for manufacturing, tuning and power handling in critical high-power devices. A hybrid scalar product, or 'overlap' integral, between the 'open' and 'closed' orthogonal basis of the open structure and the reference closed one has been defined, so introducing a figure of merit to evaluate if the derived open structure can have the same performances of the closed one in terms of fields confinement and distribution. As an example of the methodology, an 'open' version of a Gaussian horn and of a rectangular-to-circular WR10 waveguide transition have been successfully derived starting from classic 'closed' design. In order to fully test the method, the mm-wave rectangular-to-circular open-waveguide transition has been manufactured and measured (thanks to tapered close-to-open transitions and standard WR10 interfaces). The measurements well agree with full-wave numerical simulations and provide experimental validation of the proposed approach and fabrication technology. The method can be applied to other open microwave structures as well.

1 Introduction and motivation

Waveguide devices at millimetre wavelength are gaining increasing interest in many applications such as for the design of passive devices and transitions [1, 2] but also for realising horn antennas [3–5], metallic radial slotted antennas for near-field focusing applications [6], and recently for making radiators able to generate localised electromagnetic pulses [7]. In such devices, typical structure dimensions are millimetre or hundred of microns and the required tolerances make the manufacturing precision difficult to achieve and expensive. Several methods have been developed to fabricate these structures: precision milling [8, 9], lithography with subsequent electrodeposition [10], electrical discharge machining (EDM) [11], wire EDM [12] and split-block technology [13, 14]. Generally, such millimetre wave (mm-wave) devices exhibit a simply connected closed cross section and need to be fabricated out from two or several parts that can be jointed or brazed together. Here we exclude additive manufacturing fabrication techniques [2] that, although can handle peak power above 400 W, are not suitable for critical applications such as mm-wave linear particle accelerators (LINACs). The presence of the joints complicates the fabrication and increases the losses; moreover, brazed joints are not desirable in high power application since heating in the conventional brazing process modifies the copper properties increasing the breakdown probability and therefore reducing the power handling. In this paper, we focus on W-band mode couplers commonly used for the study of fundamental physics of RF breakdown in mm-wave LINACs. In particular in this context, a higher accelerating gradients [15] with low breakdown probability can be achieved thanks to RF 'open' structures [16, 17], made of two monolithic metal blocks separated by a gap that avoids high temperature brazing fabrication steps.

Finally, these structures offer the possibility of in situ tuning the RF parameters such as operating frequency, group velocity, accelerating gradient and pulse power by remotely varying the gap between the two halves. Promising techniques for fabricating mm-wave open structures have been proposed in [18–20].

In literature, an attempt to avoid metal joints is represented by the 'gap' waveguide [21, 22] based on the cut-off property of the gap formed by a perfect electrical conductor (PEC) surface and a perfect magnetic conductor (PMC) surface at a distance lower than $\lambda/4$. The cut off can be exploited by inserting a defect in the form of a groove [23], a ridge [24] or a microstrip [25]. However, the realisation of a PMC surface using quarter-wavelength long pins, other structures [26] or other symmetric electromagnetic band-gap solutions [27], introduces fabrication difficulties and additional design effort. On the other hand, if we consider only one polarisation, two simple PEC metal plates separated by a distance $< \lambda/2$ also exhibit a cut-off property since waves with the electric field parallel to the gap cannot propagate [28]. In such structure a dielectric strip of a proper dielectric constant, or a groove, can be used as defect able to eliminate the cutoff and permit wave propagation along the dielectric strip [28] or groove.

In this paper, we consider waveguide with open cross-sections (refer to Fig. 1), made by two halves with finite lateral extensions of the gap. This configuration can be seen as a particular case of the PEC parallel plate configuration when the groove-defect is derived by a standard closed cross-section waveguide. The proposed work is based on completely open structures made out from two monolithic pieces separated by a gap along with the entire structure with the aim of avoiding flanges and joins between pieces of waveguides. On the contrary, quarter-wavelength chokes are used (especially at high frequency) to guarantee a good equivalent short circuit in the junction between two consecutive standard 'closed' cross-cross section waveguides [29]. Additionally, while the quarter-wavelength RF-choke physical length depends on the working wavelength and care must be given to choose the design working frequency, in our approach, the gap lateral extend is not a critical parameter and also the gap size g has undemanding requirements, that is $g \ll \lambda$. Any open waveguide structure (i.e. a waveguide with open cross-sections, see Fig. 1), as the ones considered in this paper, supports both continuous and discrete modes; the inclusion of the continuous radiation modes in the field expansion constitutes a significant challenge for the applications of the traditional design and analysis method, e.g. the

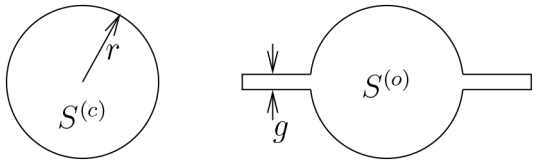

Fig. 1 *Waveguide cross-section: on the left, the closed design; on the right, the open design. The open cross-section is obtained from the closed one by deriving a gap, in the principle of infinite lateral extent, dividing the structure into two halves. In the above sketch as well as in practical implementation the lateral extent of the gap is finite and the cross-section is actually simply connected (closed)*

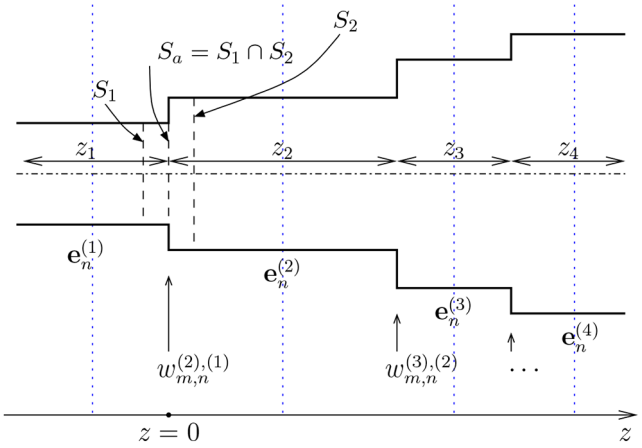

Fig. 2 *Step model of a transition. The design can be approximated with a cascade of $K-1$ step junctions and K sections*

mode matching technique (MMT), successfully applied for the analysis of closed waveguides. In our work, the field modal expansion theory [30] is extended and we verify that the conventional mode matching formulation, under suitable hypothesis, can be successfully used to describe 3D open W-band waveguide structures with general profiles. In particular, we demonstrate that, under the appropriate hypothesis, the fields of the open waveguides can be expanded in the orthonormal basis of the fields of the closed structures by introducing a negligible error. A hybrid 'overlap' integral between modes of the closed and open structures is defined and computed in order to check if the new open structures still meet the functionality and the performances of the closed ones.

The proposed methodology has been assessed starting from two mm-wave closed-waveguide designs that we converted in open ones by deriving a gap namely:

(i) A Gaussian-to-circular-TE_{11} mode converter;
(ii) A rectangular-TE_{10}-to-circular-TE_{11} transition.

The performances of the obtained open structures have been successfully verified by evaluating the above-mentioned hybrid overlap integral and by full-wave numerical simulations. Both designs can be conveniently derived by a closed one and tested in back to back configuration. While in the first design we can couple a Gaussian-beam into the open-Gaussian-horn in a free space configuration just by selecting the correct polarisation [31], for the second design it is necessary to provide a tapered transition from rectangular (standard) WR10 closed waveguide to open rectangular TE_{10} which has been fabricated for testing purposes.

The experimental scattering parameters of the open rectangular-to-circular transition have been compared with the full-wave numerical simulation.

The paper is structured as follows. In Section 2 the mode-matching method is formulated with the aim to introduce some notation valid for any closed or open design. Section 2.2 extends the mode-matching method to open waveguide structures; in this section, the new important feature of the 'hybrid' overlap integral-based analysis is presented. Moreover, guidelines to derive an open cross-section starting from the closed one are given. In Section 3 we apply and validate the proposed method on the two relevant design above-described. In Section 4, experimental measurements demonstrate that the derived open structure still retains the characteristics and the performances of the closed one. Finally, conclusions are drawn in Section 5.

2 Mode matching method formulation

Hereinafter, we briefly review the general steps adopted for the design of microwave devices with the aim to introduce some notation. It is worth noting that any smooth (open or closed) waveguide can be approximated by a cascade of $K-1$ step junctions and K sections (see Fig. 2).

2.1 Open cross section

The stepped junction of Fig. 2 can be studied with the MMT, an efficient and rigorous approach to simulate electromagnetic propagation within waveguides with discontinuities along the propagation direction. In MMT, the electromagnetic fields are decomposed into a basis set of eigenmodes, which is found by solving Maxwell's equations on each cross-section. By applying proper interface condition at discontinuities, both sides are related using a transfer matrix. The entire waveguide properties are calculated by cascading the transfer matrices. This requires to calculate the modes on both sides of the interface and their overlaps. For continuously varying structures, the scattering matrix can be obtained by discretising the structure along the z-axis.

With reference to Fig. 2, let us consider the first step junction at $z = 0$: the electromagnetic field of the (j) z_j-long and the $(j+1)$ z_{j+1}-long waveguide sections can be expressed as expansion of the N_j and N_{j+1} modes, respectively

$$\boldsymbol{E}_t^{(j)}(x,y,z) = \sum_{n=1}^{N_j} V_n^{(j)}(z)\boldsymbol{e}_n^{(j)}(x,y) \tag{1}$$

$$\boldsymbol{E}_t^{(j+1)}(x,y,z) = \sum_{m=1}^{N_{j+1}} V_m^{(j+1)}(z)\boldsymbol{e}_m^{(j+1)}(x,y)\,. \tag{2}$$

where $\boldsymbol{e}_n^{(j)}$ and $\boldsymbol{e}_m^{(j+1)}$ are the the usual modal vectors of (j)- and $(j+1)$-sections and $V_n^{(j)}$ and $V_m^{(j+1)}$ the correspondent equivalent voltages [30, 32]. In order to quantify the number N_j of modes to successfully describe each j-section, we can assess that in many

practical designs we can consider only the modal content necessary to perform the prescribed synthesis.

At the $z = 0$ junction, the continuity of the tangential electric field imposes that at the common aperture area $S_a = S_1 \cap S_2$

$$\boldsymbol{E}_t^{(j+1)} = \boldsymbol{E}_t^{(j)} \tag{3a}$$

and over the PEC $S_c = S_2 \setminus S_1$ where S_c represents the difference between the two surfaces S_2 and S_1 (as indicated in Fig. 2). The result is the step in the waveguide wall at the Section S_a.

$$\boldsymbol{E}_t^{(j+1)} = 0. \tag{3b}$$

By inserting (1) and (2) in (3a) we have:

$$V_m^{(j+1)} = \sum_{n=1}^{N_1} V_n^{(j)} w_{m,n}^{(j+1),(j)} \tag{4}$$

where

$$w_{m,n}^{(j+1),(j)} = \int_{S_a} \boldsymbol{e}_m^{(j+1)} \cdot \boldsymbol{e}_n^{(j)} \mathrm{d}S\,. \tag{5}$$

The relation (4) can be put in matrix form:

$$[V_{j+1}] = [\boldsymbol{W}] \cdot [V_j]\,. \tag{6}$$

Considering the continuity of the tangential magnetic field we obtain:

$$[I_j] = -[\boldsymbol{W}]^{\mathrm{T}} \cdot [I_{j+1}] \tag{7}$$

where I_j and I_{j+1} are the equivalent currents. Analytic formulas for the coupling coefficient (5) for rectangular/circular waveguides are available in the literature and are used in the design of structures with canonical cross section. If we approximate the slowly varing component profile in a segmented one, the scattering matrix at each discontinuity/step junction j is determined by the coupling matrix $[\boldsymbol{W}]_j$ and the overall structure scattering parameters can be derived cascading each $[\boldsymbol{S}]_j$ matrix of the step junctions, i.e. can be derived from the $[\boldsymbol{W}]_j$ matrices [32]. For the 'non-standard' open waveguides we focus in this paper, the coupling coefficients (5) should be calculated by numerical integration (see also Fig. 1). In the following we introduce an 'hybrid' overlap integral between the 'closed' and the corresponding 'open' cross-section pseudomode and we provide a way to evaluate the approximations introduced by using a standard 'closed' cross-section design in place of an 'open' one.

2.2 Mode matching method for open waveguide structures

A proper discretisation along the z axis (in K sections) and an appropriate modification of the closed cross sections into open ones (see Section 2.4), allows to exploit the similar modal contents of the two designs, leaving unaltered all the matrix $[\boldsymbol{W}]_1, [\boldsymbol{W}]_2, \ldots [\boldsymbol{W}]_{K-1}$ that describe the steps junction. Therefore, a closed design $[\boldsymbol{W}]_1^{(c)}, [\boldsymbol{W}]_2^{(c)}, \ldots [\boldsymbol{W}]_{K-1}^{(c)}$ can be converted into an open one $[\boldsymbol{W}]_1^{(o)}, [\boldsymbol{W}]_2^{(o)}, \ldots [\boldsymbol{W}]_{K-1}^{(o)}$, leaving almost unaltered the scattering matrix and junction functionality. If the modal content is almost unperturbed, this automatically guarantees similar $[\boldsymbol{W}]^{(o)}$ and $[\boldsymbol{W}]^{(c)}$ matrices.

In order to demonstrate that:

$$w_{m,n}^{(o,j+1),(o,j)} \simeq w_{m,n}^{(c,j+1),(c,j)} \tag{8}$$

we expand the open transversal mode basis, $\boldsymbol{e}_m^{(o)}$, (said hereinafter 'pseudomodes'), in the orthogonal closed basis $\boldsymbol{e}_{m'}^{(c)}$.

From (5) we have

$$\begin{aligned} w_{m,n}^{(o,j+1),(o,j)} &= \int_{S_a = S_j \cap S_{j+1}} \boldsymbol{e}_m^{(o,j+1)} \cdot \boldsymbol{e}_n^{(o,j)} \mathrm{d}S \\ &= \int_{S_a} \sum_{m'=1}^{N} a_{m,m'} \boldsymbol{e}_{m'}^{(c,j+1)} \cdot \sum_{n'=1}^{N} a_{n,n} \boldsymbol{e}_{n'}^{(c,j)} \mathrm{d}S \end{aligned} \tag{9}$$

where

$$a_{m,m'} = \int_{S_a^{(c)}} \boldsymbol{e}_m^{(o,j+1)} \cdot \boldsymbol{e}_{m'}^{(c,j+1)} \mathrm{d}S \tag{10}$$

$$a_{n,n'} = \int_{S_a^{(c)}} \boldsymbol{e}_n^{(o,j)} \cdot \boldsymbol{e}_{n'}^{(c,j)} \mathrm{d}S \tag{11}$$

are the expansion coefficients of the pseudo-mode $\boldsymbol{e}_m^{(o,i)}$ in the closed base $\boldsymbol{e}_{m'}^{(c,i)}$ for the ith waveguide.

The closed basis is not complete since it cannot represent the field in the 'open' region; however, if the closed structure has been 'carefully' opened, the field is evanescent in open regions where it decays exponentially. Therefore, if it is possible to have a one-to-one correspondence of each m' mode of the relevant modal content of the original closed structure, $\boldsymbol{e}_{m'}^{(c,j+1)}$, with a correspondent 'open' m mode we have $\boldsymbol{e}_m^{(o,j+1)} \simeq \boldsymbol{e}_{m'}^{(c,j+1)}$ and $a_{m,m'} \simeq 1$ for correspondent m an m' modes.

From (9) we have

$$\begin{aligned} w_{m,n}^{(o,j+1),(o,j)} &= \sum_{n'=1}^{N} \sum_{m'=1}^{N} a_{n,n} a_{m,m'} \int_{S_a} \boldsymbol{e}_{m'}^{(c,j+1)} \cdot \boldsymbol{e}_{n'}^{(c,j)} \mathrm{d}S \\ &= \sum_{n'=1}^{N} \sum_{m'=1}^{N} a_{n,n} a_{m,m'} w_{m',n'}^{(c,j+1),(c,j)} \end{aligned} \tag{12}$$

In matrix form:

$$[\boldsymbol{W}]^{(o,j+1),(o,j)} = [\boldsymbol{A}]^{(j+1)} [\boldsymbol{W}]^{(c,j+1),(c,j)} [\boldsymbol{A}]^{(j)} \tag{13}$$

where the $[\boldsymbol{A}]^{(\,)}$ matrices read

$$[\boldsymbol{A}]^{(\,)} = \begin{bmatrix} a_{11} & a_{12} & \cdots & a_{1N} \\ a_{21} & a_{22} & \cdots & a_{2N} \\ \cdots & & & \\ a_{N1} & a_{N2} & \cdots & a_{mN} \end{bmatrix}. \tag{14}$$

Since the basis is orthonormal, for each m-row $\sum_{m'} |a_{m,m'}|^2 < 1$ and therefore (by properly numbering correspondent modes) only $a_{m,m'}|_{m=m'} \simeq 1$ while off diagonal elements, $a_{m,m'}|_{m \neq m'}$, are negligible.

As a consequence, $[\boldsymbol{A}]^{(\,)} \simeq [\boldsymbol{I}]$ and $[\boldsymbol{W}]^{(o,j+1),(o,j)} \simeq [\boldsymbol{W}]^{(c,j+1),(c,j)}$. This results in a similar scattering matrix, $[\boldsymbol{S}]^{(o;j+1,j)} \simeq [\boldsymbol{S}]^{(c;j+1,j)}$, for the step junction between the j and $j+1$ waveguide.

In other words, provided that $a_{m,m'} \simeq 1$ in each step junction of the device, the scattering matrices of the overall device are similar namely

$$[\boldsymbol{S}]^{(o)} \simeq [\boldsymbol{S}]^{(c)}\,. \tag{15}$$

Moreover the electromagnetic field in the two devices are closely related. The similar scattering matrices guarantee that the overall functionality of the derived open device remains unaltered.

2.3 'Hybrid' overlap integral expression

The inner product (10) can be interpreted as a (virtual) coupling coefficient between the transversal modes of two different structures, namely the open structure populated by the pseudomodes $\boldsymbol{e}_{\mu t}^{(o)}$ and the closed structure with its unperturbed

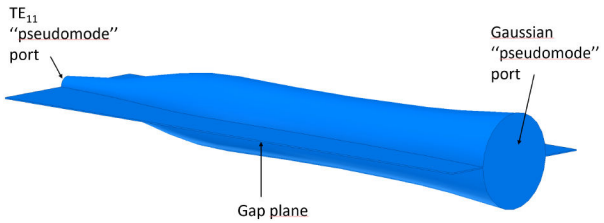

Fig. 3 *Smooth-walled Open Gaussian-TE_{11} horn converter [31]*

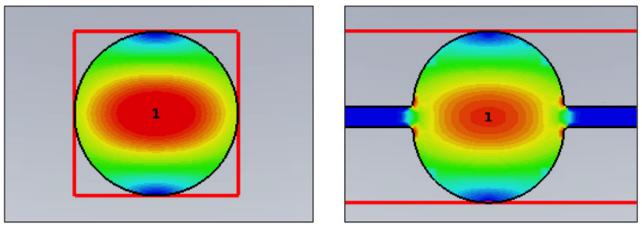

Fig. 4 *3D simulation of circular waveguide input section TE_{11} mode; on the left: closed unperturbed electric field $|E|$. on the right: open structure with slightly perturbed electric field $|E|$*

modal content $\boldsymbol{e}_{\nu t}^{(C)}$. In a more practical fashion, we define an useful and operative parameter as a two-dimensional 'overlap' integral over the cross-section of the structure

$$C_p = C_{p=\mu=\nu} = \langle \boldsymbol{e}_{\mu t}^{(O)} \cdot \boldsymbol{e}_{\nu t}^{(C)} \rangle = \int_{S = S^{(o)} \cap S^{(c)}} \boldsymbol{e}_{\mu t}^{(O)} \cdot \boldsymbol{e}_{\nu t}^{(C)*} \, \mathrm{d}S \tag{16}$$

where the superscript (c) and (o) stand for closed and open cross section, respectively (see Fig. 1) and the conjugation $*$ can be omitted if the modes are taken real.

We point out that the unity normalisation of the transversal field vectors brings the values of (16) into the $[0, 1]$ range: as the common sense suggests, if the two modes are actually identical, we obtain $C_p = 1$, on the contrary $C_p = 0$ means complete 'mode orthogonality'. Therefore, the C_p value is a metric to evaluate how much the two transverse modal fields $\boldsymbol{e}_{\mu t}^{(O)}$ and $\boldsymbol{e}_{\nu t}^{(C)}$ overlap each other.

The proposed tool is a direct application of the mode orthogonality theory [33, 34]; moreover, the C_p parameter also resembles the scattering parameters definition [35], where an eigenmode expansion of the electromagnetic fields on the ports needs to be performed in order to convert an electric field pattern on a port to a scalar complex number corresponding to the voltage.

2.4 Guidelines to derive an open cross section

Hereinafter we list the rules to optimally convert an mm-wave closed structure into an open one

(i) The electromagnetic field inside a waveguide is associated with its current distribution $\boldsymbol{J}_s$ over the boundary surfaces S of the guide. Let be $\hat{\boldsymbol{n}}$ the unit vector orthogonal to S towards outside S. Let the following $\boldsymbol{J}_s = \boldsymbol{H} \times \hat{\boldsymbol{n}}$ the surface current density. It is true that a portion of the metallic structure can be removed if a narrow slot is cut in the wall such that its long dimension runs along the current line or along a region of the wall where the $\boldsymbol{J}_s$ is zero. In fact, this produces only a minor perturbation of the current distribution and a very little coupling of the internal field to external space. On the other hand, a slot cut in the wall radiates to space only if the gap cuts across current lines of $\boldsymbol{J}_s$ corresponding to the considered mode.

Therefore, for each mode in the structure, we can observe only the surface currents. The non-radiating slots theory [36, p. 287] can be used for the purpose of this work because it offers a method to establish where the gap of our open structure can be done.

(ii) Since the gap breaks the waveguide rotation symmetry, it is necessary to choose its orientation with respect to the polarisation of the modal vectors in the modal content. In many cases, only one plane can be chosen as a cut plane since only one orientation maximises the inner product (16). We can read the inner product as a tool to select the correct relative orientation of the gap with respect to the polarisation of the modal content.

(iii) Concerning the gap size g (see Fig. 1), in analogy to the behaviour observed in NonRadiative (NR) waveguides [28, 37], we apply the NR criterion which basically prevents the propagation of the radiation outside the interested central region; in particular, for g sensibly lower than $\lambda/2$, where λ is the operative wavelength, the NR condition is well verified and the evanescent field outside the central region decreases very rapidly. On the contrary, when g approaches $\lambda/2$ the confinement mechanism becomes weaker and weaker and the mode extends well beyond the central region resulting in radiation losses.

It is worth to note that only the hybrid scalar product (16) gives a quantitative figure of merit to mathematically evaluate the 'distance' between the open structure and the reference one as well as a way to predict that the functionality of the device is preserved, as it will be demonstrated with two examples in the following section.

3 Numerical results

In this section we test the proposed method with numerical calculations on two open mm-wave structures: (1) a Gaussian-TE_{11} mode converter and (2) a rectangular-to-circular waveguide transition. Our strategy consists of firstly following the guidelines of Section 2.4 in order to derive the gap in the geometry and obtain open structures with unaltered functionality. Then, we calculate the C_p integrals in order to quantitatively verify that (8) holds. Finally, we compare the scattering parameters between the closed and the open structures.

3.1 Open TE_{11}-Gaussian horn converter

Starting from the closed structure, it is possible to derive tha gap by inserting the 'Gap plane' between the two halves. Fig. 3 shows the resulting geometry of open Gaussian-TE_{11} horn obtained by following the guidelines in Section 2.4. In particular, we include a gap plane having a gap size $g = 0.4\,\mathrm{mm} \simeq 0.15\lambda$. The simulated domain is a region of vacuum surrounded by a PEC. In Fig. 4 it is possible to observe that the fundamental TE_{11} mode of the closed and the open circular waveguide input section remains mostly unaltered confirming that the opening cut is optimally operated.

The presence of the gap could in principle lead to several problems: other modes could propagate because the waveguide is overmoded or oversized [34]; the Gaussian horn converter could couple power to other modes than the desired one and any discontinuities in the waveguide could cause mode conversion

Table 1 Calculated C_p for TE_{11}-Gaussian horn converter

Section	$C_{TM_{11}}^{(O),(C)}$	$C_{TE_{11}}^{(O),(C)}$
r_{min}	0.9240	0.9600
r_{max}	0.9873	0.9944

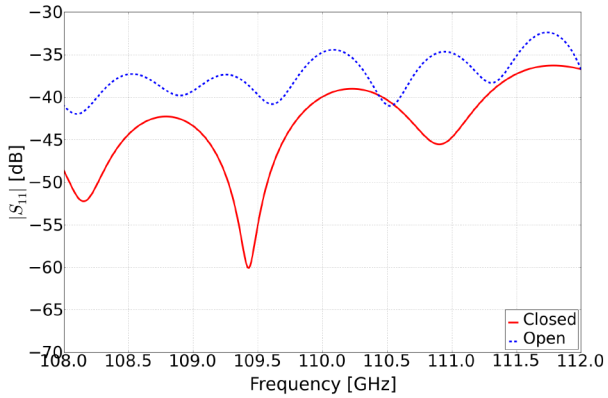

Fig. 5 *Simulated reflection coeffient $|S_{11}|$ for the open and closed Gaussian-TE_{11} horn converter*

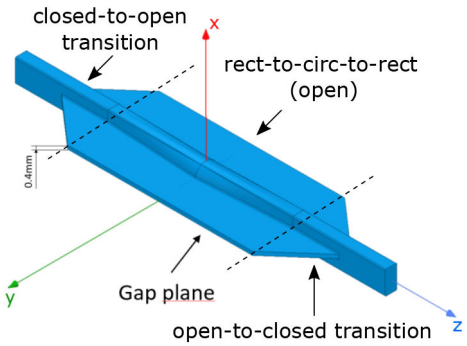

Fig. 6 *Rectangular-to-circular-to-rect open waveguide transition. Input closed-to-open and output open-to-closed tapered transition have been designed and included for testing purposes*

which increases attenuation. So, in order to quantitatively appreciate the correct conversion of the closed structure to the open one, we compute the C_p parameter (16). For the TE_{11}-Gaussian horn converter, considering that the relevant modal content is limited only to two modes (since it is well known that the Gaussian mode can be obtained as a mode mixture of two modes, 85% TE_{11} and 15% of TM_{11} [3]), the $[\boldsymbol{A}]$ matrix of the generic j-section becomes:

$$[\boldsymbol{A}] = \begin{bmatrix} C_{TM_{11}}^{(O),(C)} & \simeq 0 \\ \simeq 0 & C_{TE_{11}}^{(O),(C)} \end{bmatrix} \tag{17}$$

In Table 1 we report the value of $C_{TM_{11}}^{(O),(C)}$ $C_{TE_{11}}^{(O),(C)}$ for two representative sections of the step model (the section at the smallest radius $r_{min} = 1.5\,\text{mm}$ and at the largest one $r_{max} = 7.53\,\text{mm}$). For the calculation of the C_p values, modes have been extracted from 2D numerical simulation, thus a 2D eigenmode solver is needed in order to obtain the electric fields $\boldsymbol{e}_{\mu t}^{(O)}$ and $\boldsymbol{e}_{\nu t}^{(C)}$ for the TM_{11} and the TE_{11} mode of the considered section for the open and closed structure. For example, to compute $C_{TM_{11}}^{(O),(C)}$ we have:

$$C_{TM_{11}}^{(O),(C)} = \langle \boldsymbol{e}_{TM_{11}t}^{(O)} \cdot \boldsymbol{e}_{TM_{11}t}^{(C)} \rangle = \int_{S = S^{(O)} \cap S^{(C)}} \boldsymbol{e}_{TM_{11}t}^{(O)} \cdot \boldsymbol{e}_{TM_{11}t}^{(C)*} \, \mathrm{d}S \tag{18}$$

Being $C_{TM_{11}}^{(O),(C)} \simeq 1$ and $C_{TE_{11}}^{(O),(C)} \simeq 1$ in each i-section of the step model, we can assert that $[\boldsymbol{W}]^{(O)} \simeq [\boldsymbol{W}]^{(C)}$. This demonstrates that the open structure still fulfils the same requirements of the closed one.

The obtained matrix (17) at $r = r_{max}$ is

$$[\boldsymbol{A}]_{r = r_{max}} = \begin{bmatrix} 0.9873 & 0.022 \\ 0.007 & 0.9944 \end{bmatrix} \simeq [\boldsymbol{I}] \tag{19}$$

The obtained open structure has been also tested by comparing the scattering parameters with respect to the original structure. From Fig. 5 it is evident that the $|S_{11}|$ trend is only slightly deteriorated from the presence of the gap, still keeping the open Gaussian antenna well-adapted in the operative frequency range.

3.2 Rect-to-circ waveguide transition

For the second closed structure, it is also possible to derive a gap by inserting a 'gap plane' of thickness $g = 0.4\,\text{mm} \simeq 0.15\lambda$ between the two halves. The simulated domain is a region of vacuum surrounded by a PEC. Fig. 6 shows the geometry of the rect-to-circ transition in back-to-back configuration (rect-to-circ-to-rect). For testing purpose, a closed-rect-to-open-rect and an open-rect-to-closed-rect transition have been added as input and output sections respectively.

For this structure the modal content is limited to the fundamental mode of each section considered. On the middle section $(x, y, z = 0)$ we have a circular cross section with radius $r = 1.195\,\text{mm}$ and the $C_{TE_{11}}^{(O),(C)} = 0.9944$ has been obtained showing that the opening cut is optimally operated. In Table 2 we report the value of the hybrid scalar product (overlap integral) between the 'target' analytical mode and the actual numerical field, i.e. we compute a C_p parameter by overlapping the analytical $C_{TE_{11}}^{(a)}$ with

Table 2 Calculated C_p for TE_{11}-mode mm-wave transition

$C_{TE_{11}}^{(a),(c)}$	$C_{TE_{11}}^{(a),(o)}$	$C_{TE_{11}}^{(c),(o)}$
0.9999	0.9944	0.9944

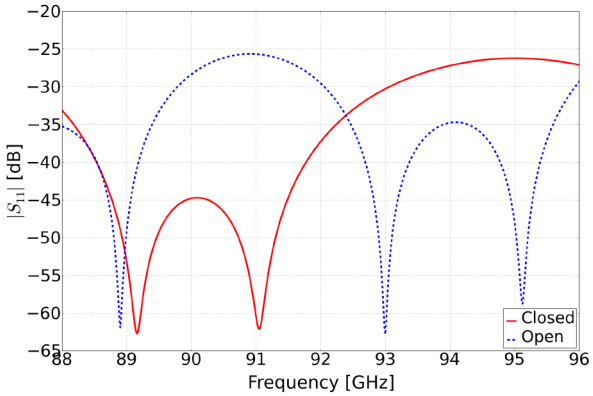

Fig. 7 *Simulated reflection coeffient $|S_{11}|$ for the open and closed stand-alone structure*

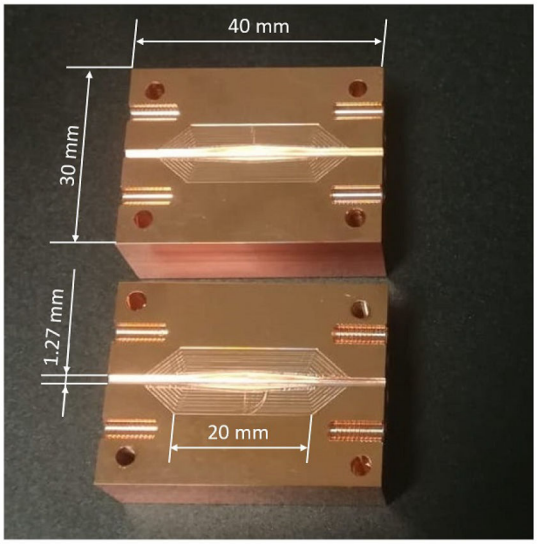

Fig. 8 *Open mm-wave WR10 waveguide stand-alone structure*

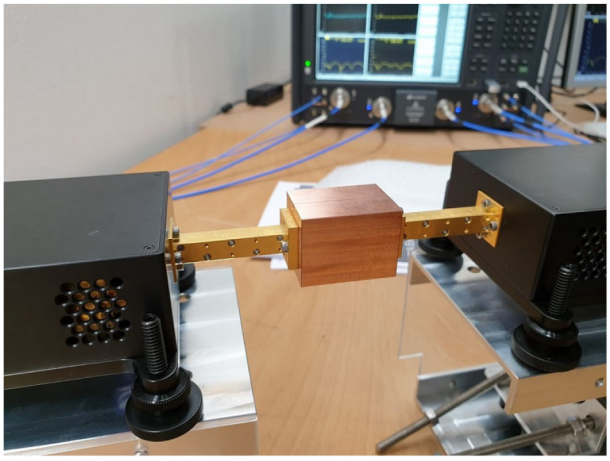

Fig. 9 *Experimental measurement setup*

the simulated closed and open circular mode of the mm-wave WR10 transition.

In the initial/final section we have a rectangular cross section (input/output rectangular waveguide) and the $C_{TE_{10}}^{(O),(C)}$ coefficient is 0.969

In a transition section, the rectangular waveguide gradually transforms into the circular one and the cross-section assumes various shapes. So we can assert that, in each cross-section, $[\boldsymbol{W}]^{(o)} \simeq [\boldsymbol{W}]^{(c)}$ demonstrating that the open structure still fulfils the same requirements of the closed one. Fig. 7 shows the comparison between the simulated scattering parameters of the two structures. It is evident that the $|S_{11}|$ trend is only slightly shifted in frequency due to the presence of the gap, still keeping the open structure well-adapted in the operative frequency range.

4 Experimental results

A prototype of the open rect-to-circ transition – described in Section 3.2 – has been manufactured, it is made of two separated copper halves machined by milling with a tolerance of $\pm 2\,\mu m$ and a surface roughness $< 80\,nm$ by Comeb S.r.l. [38]. The manufactured prototype also includes an input and output tapered transitions from the standard closed WR10 waveguide to the open ones. Fig. 8 shows a photograph of the realised mm-wave open structure with the geometric dimensions in detail. The experimental measurement have been carried out by means of a 4-port Keysight N5245B PNA-X microwave network analyser and two W-band Keysight N5262BW10-STD Transceiver modules (Tx/Rx) by Virginia diodes. The experimental setup is shown in Fig. 9. Fig. 10 shows the experimental *S*-parameters of the prototype compared to the simulation results. The return loss of the mm-wave open structure is well matched inside the operating bandwidth and the

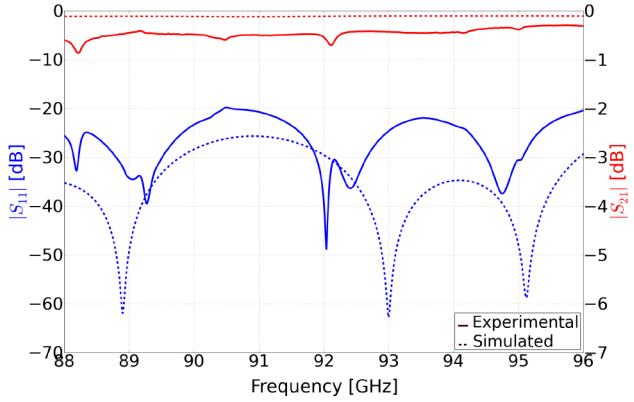

Fig. 10 *Experimental versus simulated reflection and transmission coefficients of the open rect-to-circ transition*

insertion loss results in agreement with the simulated data with a discrepancy not larger than 0.7 dB. These small differences may be due to misalignment from manufacturing tolerances and to not perfect mechanical coupling between the surfaces. In order to confirm this, some simulations have been performed, where a shift on the gap-plane (*yz*) along *y*-direction between the two halves-pieces has been introduced. Fig. 11*a* confirms that a 25 µm of misalignment produces a down-shift of the $|S_{11}|$ (the 'simulated misalignment' red-dashed curve) and a deterioration especially around 92 GHz, observed also in the experimental results (black solid line). This simulated misalignment – which represents the more likely experimental scenario – gives rise to some dips in the simulated $|S_{21}|$ clearly visible in the red-dashed curve of Fig. 11*b* and already observed in the $|S_{21}|$ measurement (black solid line).

We deem these error could be reduced by inserting a series of screws and alignment dowels along the milling path [39]. It is worth to note that two closed-to-open transitions have been included for testing the above-described prototype. Conversely, no screws are needed in all-open design where micro-precision translation stages could allow to accurately control and optimise the position of the two separate and movable halves.

5 Conclusion

We presented a methodology, based on the field modal expansion theory, to analyse mm-wave open components for W-band particle accelerators. The proposed method gives some important guidelines in order to optimally derive the open structure from a well-designed closed one. Moreover, the conventional MMT has been extended for the case at hand and a useful parameter has been defined as an 'overlap' integral to measure the degree of perturbation of the so obtained open device. This tool acts as a 'mode control' to verify if the propagation in a well-defined pattern can be maintained in the open structure. Finally, finite element method simulations have been performed and compared to experimental measurements to further confirm the effectiveness of the proposed tool as well as the advantages of the 'open" configuration from the fabrication point of view. The above methodology has been successfully applied to derive open structures that still fulfil the required mode conversion and function of the original ones. The general formulation of the proposed method strongly reduces design effort and it is valid for any application where open structures can be suitable.

6 Acknowledgments

This work was supported by E. Nanni, M. Dal Forno, J. Neilson and S. Tantawi from SLAC National Accelerator Laboratory are gratefully acknowledged for having provided the closed Gaussian-horn design.

7 References

[1] Isapour, A., Kouki, A.: 'Vertical LTCC integrated rectangular waveguide and transitions for millimeter-wave applications', *IEEE Trans. Microw. Theory Tech.*, 2019, **67**, (3), pp. 868–882

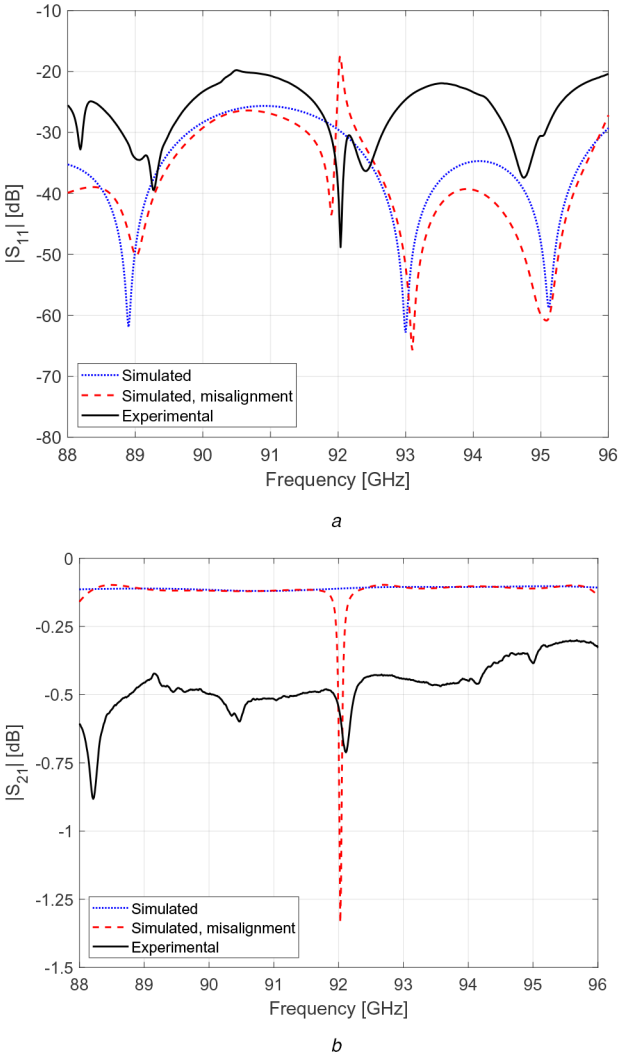

Fig. 11 *S-parameters of the open rect-to-circ transition when a misalignment between the two halves is introduced in the simulated geometry. The red-dashed curves represent the simulation results in presence of the shift. For the sake of comparison, we have kept in the figure the experimental and the simulated (without any misalignment) results*
(a) Reflection $|S_{11}|$ coefficients, ***(b)*** Transmission $|S_{21}|$ coefficients

[2] Manafi, S., Al-Tarifi, M., Filipovic, D.S.: 'Millimeter-wave double-ridge waveguide and components', *IEEE Trans. Microw. Theory Tech.*, 2018, **66**, (11), pp. 4726–4736
[3] Gonzalo, R., Teniente, J., del Rio, C.: 'Improved radiation pattern performance of Gaussian profiled horn antennas', *IEEE Trans. Antennas Propag.*, 2002, **50**, (11), pp. 1505–1513
[4] Dong, B., Yang, J., Dahlström, J., *et al.*: 'Optimization and realization of quadruple-ridge flared horn with new spline-defined profiles as a high-efficiency feed for reflectors over 4.6–24 GHz', *IEEE Trans. Antennas Propag.*, 2017, **67**, 585–590
[5] Manshari, S., Koziel, S., Leifsson, L.: 'A wideband corrugated ridged horn antenna with enhanced gain and stable phase center for X- and Ku-band applications', *IEEE Antennas Wirel. Propag. Lett*, 2019, **18**, (5), pp. 1031–1035
[6] Pavone, S.C., Ettorre, M., Albani, M.: 'Analysis and design of bessel beam launchers: longitudinal polarization', *IEEE Trans. Antennas Propag.*, 2016, **64**, (6), pp. 2311–2318
[7] Comite, D., Fuscaldo, W., Pavone, S., *et al.*: 'Propagation of nondiffracting pulses carrying orbital angular momentum at microwave frequencies', *Appl. Phys. Lett.*, 2017, **110**, (11), p. 114102
[8] Dal Forno, M.: 'Design of a high power TM01 mode launcher optimised for manufacturing by milling'. Tech. Rep., SLAC National Accelerator Lab., Menlo Park, CA (United States), 2016. Available at http://www.osti.gov/scitech/servlets/purl/1336365
[9] Dal Forno, M., Dolgashev, V., Bowden, G., *et al.*: 'RF breakdown tests of mm-wave metallic accelerating structures', *Phys. Rev. Accel. Beams*, 2016, **19**, p. 011301
[10] Henke, H.: 'Planar structures for electron acceleration'. Proc. Particle Accelerator Conf., Dallas, TX, 1995, vol. 37, pp. 1750–1752
[11] Hill, M.E., Lin, X.E., Callin, R.S., *et al.*: 'Planar dielectric accelerator structures at W band'. Tech. Rep., SLAC National Accelerator Lab., Menlo Park, CA (United States), 2000

[12] Henke, H.: 'Millimeter-wave structures and power sources'. Proc. European Particle Accelerator Conf., Vienna, Austria, 2000, pp. 202–206
[13] Koenen, C., Siart, U., Eibert, T.F., *et al.*: 'A configurable coupling structure for broadband millimeter-wave split-block networks', *IEEE Trans. Microw. Theory Tech.*, 2015, **63**, (12), pp. 3954–3961
[14] Shang, X., Penchev, P., Guo, C., *et al.*: '*W*-band waveguide filters fabricated by laser micromachining and 3-D printing', *IEEE Trans. Microw. Theory Techn.*, 2016, **64**, (8), pp. 2572–2580
[15] Dolgashev, V.A., Tantawi, S.G., Spataro, B.: 'Study of basic RF breakdown phenomena in high gradient vacuum structures'. Proc. Linear Accelerator Conf., LINAC2010, Tsukuba, Japan FR105, 2010
[16] Dal Forno, M., Dolgashev, V., Bowden, G., *et al.*: 'Electron beam excitation of a surface wave in mm-wave open accelerating structures'. Proc. Seventh Int. Particle Accelerator Conf. (IPAC 2016), Busan, Korea, 8–13 May 2016
[17] Dal Forno, M., Dolgashev, V., Bowden, G., *et al.*: 'Experimental measurements of RF breakdowns and deflecting gradients in mm-wave metallic accelerating structures', *Phys. Rev. Accel. Beams*, 2016, **19**, p. 051302. Available at https://link.aps.org/doi/10.1103/PhysRevAccelBeams.19.051302
[18] Henke, H.: 'Mm-wave LINAC and wiggler structures'. Proc. Fourth European Particle Acc. Conf., 1994, pp. 322–326
[19] Henke, H., Merte, R., Nassiri, A., *et al.*: 'Millimeter-wave RF structure'. Proc. 18th Int. Linear Accelerator Conf., CERN, Geneva, 1996, p. 524, Internal report 96-07
[20] Bruns, W.: 'Design of input couplers and endcells for side coupled muffin-tin structures'. Proc. Particle Accelerator Conf., Dallas, TX, USA., vol. 2, May 1995, pp. 1088–1089
[21] Kildal, P.-S., Alfonso, E., Valero-Nogueira, A., *et al.*: 'Local metamaterial-based waveguides in gaps between parallel metal plates', *IEEE Antennas Wirel. Propag. Lett.*, 2009, **8**, pp. 84–87
[22] Berenguer, A., Fusco, V., Zelenchuk, D.E., *et al.*: 'Propagation characteristics of groove gap waveguide below and above cutoff', *IEEE Trans. Microw. Theory Tech.*, 2016, **64**, (1), pp. 27–36
[23] Farahbakhsh, A., Zarifi, D., Zaman, A.U.: '60-GHz groove gap waveguide based wideband *H*-plane power dividers and transitions: for use in high-gain slot array antenna', *IEEE Trans. Microw. Theory Tech.*, 2017, **65**, pp. 4111–4121
[24] Fan, F., Yang, J., Vassilev, V., *et al.*: 'Bandwidth investigation on half-height pin in ridge gap waveguide', *IEEE Trans. Microw. Theory Tech.*, 2017, **66**, 100–108
[25] Valero-Nogueira, A., Baquero, M., Herranz, J.I., *et al.*: 'Gap waveguides using a suspended strip on a bed of nails',*IEEE Antennas Wirel. Propag. Lett.*, 2011, **10**, pp. 1006–1009
[26] Rajo-Iglesias, E., Kildal, P.-S.: 'Numerical studies of bandwidth of parallel-plate cut-off realised by a bed of nails, corrugations and mushroom-type electromagnetic bandgap for use in gap waveguides', *IET Microw. Antenna P.*, 2011, **5**, (3), pp. 282–289
[27] Ebrahimpouri, M., Quevedo-Teruel, O., Rajo-Iglesias, E.: 'Design guidelines for gap waveguide technology based on glide-symmetric holey structures', *IEEE Microw. Wirel. Compon. Lett.*, 2017, **27**, 542–544
[28] Yoneyama, T., Nishida, S.: 'Nonradiative dielectric waveguide for millimeter-wave integrated circuits', *IEEE Trans. Microw. Theory Tech.*, 1981, **29**, (11), pp. 1188–1192
[29] Yevdokymov, A., Kryzhanovskiy, V., Pazynin, V., *et al.*: 'Ka-band waveguide rotary joint', *IET Microw. Antennas Propag.*, 2013, **7**, (5), pp. 365–369
[30] Conciauro, G.: '*Introduzione alle onde elettromagnetiche*' (McGraw-Hill, Milano, Italy, 1994, 2nd edn.)
[31] Torrisi, G., Sorbello, G., Leonardi, O., *et al.*: 'Closed-to-open conversion of a mm-wave Gaussian horn antenna'. 12th European Conf. Antennas and Propagation (EuCAP 2018), 2018
[32] Conciauro, G., Guglielmi, M., Sorrentino, R.: '*Advanced modal analysis: CAD techniques for waveguide components and filters*' (John Wiley & Sons Inc, New York, USA., 2000)
[33] Someda, C.: '*Electromagnetic waves*' (CRC Press, Boca Raton, FL, USA., 2006, 2nd edn.)
[34] Mahmoud, S.: '*Electromagnetic waveguides: theory and applications*', Ser. Electromagnetics and Radar Series (Peregrinus, Stevenage, UK., 1991)
[35] Comsol, COMSOL RF Module Users' Guide, COMSOL Multiphysics®
[36] Silver, S.: '*Microwave antenna theory and design*', Ser. radiation laboratory series (McGraw-Hill Book Company, New York, USA., 1949)
[37] Yoneyama, T., Tozawa, N., Nishida, S.: 'Loss measurements of nonradiative dielectric waveguide (special papers)', *IEEE Trans. Microw. Theory Techn.*, 1984, **32**, (8), pp. 943–946
[38] 'Comeb s.r.l., via dei Ranuncoli snc, 00134 Roma, www.comeb.it'
[39] Furtula, V., Salewski, M.: 'W-band waveguide bandpass filter with E-plane cut', *Rev. Sci. Inst.*, 2014, **85**, (7), p. 074703. Available at https://doi.org/10.1063/1.4889875